

Competing mechanism driving diverse pressure dependence of thermal conductivity of $X\text{Te}$ ($X = \text{Hg}, \text{Cd}, \text{and Zn}$)

Tao Ouyang^{1,*} and Ming Hu^{1,2,†}¹*Institute of Mineral Engineering, Division of Materials Science and Engineering, Faculty of Georesources and Materials Engineering, RWTH Aachen University, 52064 Aachen, Germany*²*Aachen Institute for Advanced Study in Computational Engineering Science (AICES), RWTH Aachen University, 52062 Aachen, Germany*

(Received 24 September 2015; revised manuscript received 19 November 2015; published 14 December 2015)

Effectively engineering the lattice thermal conductivity of materials is a key interest of the current thermal science community. Pressure or compressive strain is one of the most worthwhile processes to modify the thermal transport property of materials, due to its robust tunability and flexibility of realization. While it is well documented in the literature that the application of hydrostatic pressure normally increases the thermal conductivity of bulk materials, little work has been performed on abnormal pressure-dependent thermal conductivity and the governing mechanism has not been fully understood yet. In this paper, taking bulk telluride systems $X\text{Te}$ ($X = \text{Hg}, \text{Cd}, \text{Zn}$) as examples, we show, by combining first-principle calculation and the phonon Boltzmann transport equation, that the thermal conductivity presents diverse pressure dependence although they belong to the same group. The thermal conductivity of ZnTe is independent of pressure, while abnormal negative pressure dependence of thermal conductivity is observed in HgTe . As for CdTe , the trend falls in between HgTe and ZnTe and relies largely on the temperature. By comparing the key contributors of the lattice thermal conductivity, we find that the diverse pressure dependence of the lattice thermal conductivity is governed by the competition between the enhancement of group velocity of longitudinal acoustic and optic modes and the reduction of phonon relaxation time of transverse acoustic modes, with both effects being fully quantified by our calculation. Comparison with traditional bulk systems such as silicon further underpins the governing mechanism. The correlation between the diverse thermal transport phenomena and the nature of the atomic bonding is also qualitatively established. These findings are expected to deepen our understanding of manipulating phonon transport of bulk materials via simple compressive strain and are also helpful for related applications, such as optimizing thermoelectric performance.

DOI: [10.1103/PhysRevB.92.235204](https://doi.org/10.1103/PhysRevB.92.235204)

PACS number(s): 63.20.kg, 63.20.dk, 84.60.Rb, 66.70.Df

I. INTRODUCTION

It is well known that lattice thermal conductivity is a fundamental physical property of materials and also an important parameter for design in a wide range of technology and engineering applications [1–4]. How to effectively modulate the thermal conductivity of materials plays a critical role in the current thermal transport research community, in areas such as thermoelectrics [1], heat dissipation [2], thermal insulators [3], and thermal management [4]. So far, great efforts have been adopted to manipulate the thermal transport via doping, generating defects, varying the phonon band structure, or coupling with a substrate [5–13]. These processes indeed have made headway in this subject and promote the development of relative thermal transport research.

In addition to these methods, pressure (more generally speaking, mechanical strain) is also an effective way to engineer the lattice thermal conductivity [14–24]. Owing to the flexibility and easy realization in experiments, this approach has attracted tremendous interest from both theoretical and technological aspects. Ross *et al.* make a comprehensive experimental review of the pressure effect on the thermal conductivity and conclude that pressure will enhance the

thermal conductivity of covalent and semiconducting materials [14]. Using the transient heating technique, Goncharov *et al.* experimentally investigated the thermal transport in compressed argon and found a power-law increase in thermal conductivity with compression increasing [15]. Employing density functional theory (DFT) calculations or the Green-Kubo molecular dynamics (GKMD) method, a similar trend has been presented theoretically in iron [16], argon [17,18], diamond [19], silicon [20], cubic boron nitride [21], and also for some nanostructures [22–24]. If one makes a statistical analysis of the above results, a universal conclusion seems to be drawn—that the pressure usually plays a positive effect on the lattice thermal conductivity of bulk materials.

However, negative pressure effect on the thermal transport property was also reported recently [25]. From the aspect of first-principle calculation, Parrish *et al.* show that the room temperature thermal conductivity of bulk silicon is almost a constant under compression [17], which is quite different from that found by the previous classical MD simulations [20]. Utilizing the time-domain thermoreflectance approach, Hohensee *et al.* observe this unique thermal transport behavior before the phase transition of silicon [25]. Lindsay *et al.* calculate the binary compound materials and declare that the thermal conductivity of the compounds generally decreases with pressure when the compounds are composed of two masses with large mass ratio [26]. These studies of the thermal transport phenomena indicate that pressure, which was originally thought to enhance the thermal conductivity, is not a universal trend for all bulk materials. Therefore, it is intuitive to speculate that there might exist some underlying

*On leave from Hunan Key Laboratory for Micro-Nano Energy Materials and Devices and Department of Physics, Xiangtan University, Xiangtan 411105, Hunan, China.

†Author to whom correspondence should be addressed: hum@ghi.rwth-aachen.de

physical mechanisms governing the positive or negative effect of pressure on the lattice thermal conductivity.

In this paper, based on first-principle calculations we present a systematic study of the pressure effect on the lattice thermal conductivity of bulk telluride systems $X\text{Te}$ ($X = \text{Hg}, \text{Cd}, \text{Zn}$), all of which are promising thermoelectric materials [27]. Our results show that, although the three materials belong to the same group, their thermal conductivity possesses fully different pressure dependence, which mainly depends on the competition between the enhancement of group velocity of longitudinal acoustic and optic modes and the reduction of phonon relaxation time of transverse acoustic modes. The remainder of the paper is organized as follows. In Sec. II, a brief description about the Peierls-Boltzmann transport equation (PBTE) method and our first-principle calculation is given. In Sec. III, we present the pressure effect on the thermal conductivity of HgTe, CdTe, and ZnTe in sequence. To interpret the diverse pressure-dependent thermal transport phenomena, the physical parameters at the phonon mode level, e.g., phonon group velocity, phonon lifetime, Grüneisen parameters, are analyzed. In addition, an understanding about the pressure-dependent thermal conductivity is developed in Sec. IV and the behavior is correlated with the nature of the interatomic interaction in different structures. Finally, our concluding remarks are summarized in Sec. IV.

II. COMPUTATIONAL DETAILS

At ambient conditions, $X\text{Te}$ ($X = \text{Hg}, \text{Cd}, \text{Zn}$) crystal has a zinc-blende structure (space group $F4\bar{3}m$) with two basis atoms per primitive cell. Previous experiments have demonstrated that the pressure induced phase transitions for HgTe, CdTe, and ZnTe are about 1.5, 3.5, and 9.0 GPa, respectively [28–31]. In this work we mainly focus on the pressure effect (≤ 1.5 GPa, lower than the phase transition pressure) on the thermal transport properties of $X\text{Te}$ with the zinc-blende phase; therefore the detailed process of phase transition and the corresponding phonon mode softening is not taken into consideration. For the isotropically cubic systems examined in this work, the thermal conductivity is a scalar and can be expressed as

$$\kappa = \kappa_{xx} = \frac{1}{V} \sum_{\lambda} C_{\lambda} v_x^2 \tau_{\lambda x}, \quad (1)$$

where V is the crystal volume, C_{λ} the mode specific heat, and v_x the group velocity along x . Here we use the shorthand $\lambda = (j, \vec{q})$, where j and \vec{q} are phonon branch and wave vector, respectively. $\tau_{\lambda x}$ is the phonon lifetime obtained from the nonequilibrium phonon distribution [32,33]. In this calculation, we use a full Brillouin zone and iterative solution of the Peierls-Boltzmann transport equation as implemented in the SHENGBTE package [34]. The only inputs are harmonic and anharmonic interatomic force constants (IFCs), which are obtained from first principles.

Our first-principle calculations are carried out with the Vienna Ab Initio Simulation Package (VASP) [35]. The Ceperley-Alder local-density approximation (LDA) is adopted for exchange and correlation function [36]. Projector augmented wave (PAW) pseudopotentials are used for the interaction among atoms [37] and the kinetic energy cutoff for the

plane-wave basis is set to 500 eV. The Brillouin zone of the primitive cell is sampled with $15 \times 15 \times 15$ Monkhorst-Pack k mesh. During the structure optimizations, both the atom positions and lattice constants are fully relaxed until the maximum force acting on each atom is less than 10^{-5} eV/Å. The relaxed lattice parameter is 6.447, 6.421, and 6.003 Å for HgTe, CdTe, and ZnTe, which agrees very well with the experimental data of 6.453, 6.482, and 6.101 Å [38]. To obtain the IFCs, a $5 \times 5 \times 5$ supercell is constructed, where the numbers of k mesh used are accordingly scaled down compared with the case of unit cell calculation. The size of the supercell (250 atoms) is far larger than the cutoff interaction of the third-order force constant and similar treatment has also been extensively used in previous papers [17,19,26,34,39]. When dealing with the third-order anharmonic IFCs, the translational invariance constraint is enforced via using the Lagrangian multiplier method [40]. As for the interaction cutoff of the third-order force constant, we have done the convergence test (the results are not shown here for brevity) and found that the thermal conductivity changes obviously in the small cutoff region ($<$ third-nearest neighbors), while it stays almost unchanged when the cutoff is larger than third-nearest neighbors. Therefore, taking into consideration the computational accuracy and the time-consuming calculations, the fourth-nearest neighbors are chosen as the interaction cutoff for the third-order force constant in this work. The convergence of thermal conductivity with respect to the phonon q -grid size is also tested in our calculation. The results show that the thermal conductivity (at room temperature 300 K) of HgTe gradually reaches a stable value, when the phonon q grid increases from $23 \times 23 \times 23$ to $25 \times 25 \times 25$, and the difference between the two-phonon q grids is less than 5%, which indicates the convergence of the BTE calculation. For keeping the computations consistent, we use the $25 \times 25 \times 25$ phonon q grid for all of our calculations. Conservation of energy in the three-phonon processes is enforced by the Dirac delta distributions with locally adaptive Gaussian approximation (scale parameter for broadening is chosen as 1.0) [41].

III. RESULTS AND DISCUSSION

A. HgTe

Through solving the eigenvalues of the dynamical matrix constructed via the harmonic IFCs, we first obtain the phonon dispersion curves of HgTe as shown in Fig. 1(a). It can be found that the calculated phonon branches of HgTe under

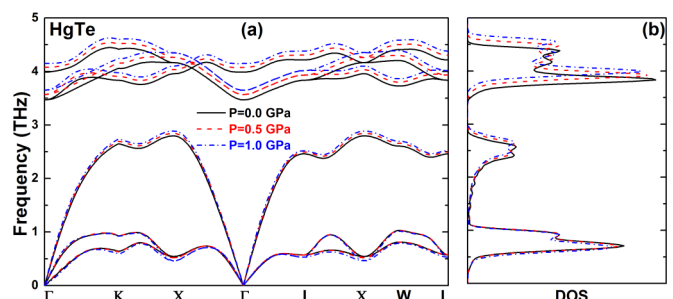


FIG. 1. (Color online) (a) The phonon spectra of HgTe under different pressures and (b) corresponding phonon density of state (DOS).

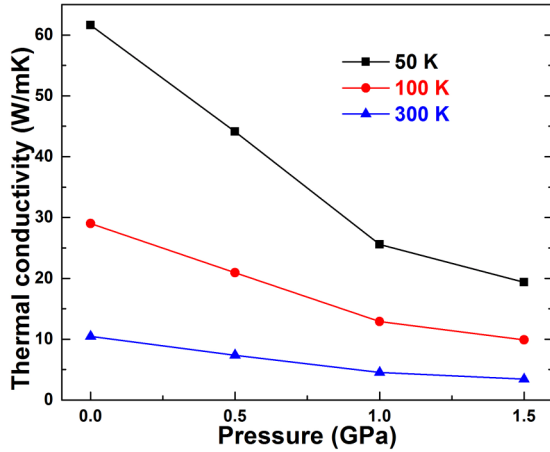


FIG. 2. (Color online) The lattice thermal conductivity of HgTe as a function of pressure at three typical temperatures.

zero pressure are in good agreement with previous theoretical and experimental studies [42,43]. For example, the frequency of the transverse optic phonon mode (TO) at the Γ point is about 3.47 THz and the experimental measured value is about 3.54 THz. This accurate phonon band structure validates the reliability of the IFCs obtained in this work. Meanwhile, we should note here that the real space supercell approach [44] cannot directly provide the splitting between the longitudinal and transverse optic phonon modes. Therefore, the Born effective charges and dielectric constants are taken into account in our calculation [45,46]. Under the pressure, one can see that the two low-frequency transverse acoustic (TA) phonon branches become softer around the X and K points. As for the longitudinal acoustic (LA) and optic phonon branches, they gradually shift to high frequencies, analogous to that observed in most bulk materials such as diamond and solid argon [17–19]. From the phonon density of state shown in Fig. 1(b) we can also see this change more clearly.

The lattice thermal conductivity of HgTe as a function of pressure at three typical temperatures is plotted in Fig. 2. Owing to the enhancement of intrinsic phonon scattering, it can be seen that the thermal conductivity decreases as the temperature increases from 50 to 300 K. At room temperature (300 K) the calculated thermal conductivity (0.0 GPa) is about 10.46 W/mK, which is higher than the experimental measurement (standard atmospheric pressure) of about 2.14 W/mK [47]. That is to say, our calculations overestimate the thermal conductivity of HgTe. However, this overestimation is understandable considering that, in the temperature range we are interested in, the defect (e.g., impurity, grain boundary, and dislocation) induced phonon scattering in the experimental samples [47] plays significant roles as compared with the intrinsic phonon-phonon scattering. On the other hand, it should be noted here that although our result overestimates the thermal conductivity, in this work we mainly focus on the qualitative response of the thermal transport property to the external pressure, rather than the accurate absolute value of the lattice thermal conductivity. Upon compression, we can notice that the thermal conductivity of HgTe decreases remarkably at the three typical temperatures considered here. At 1.5 GPa, the thermal conductivity at room temperature is

reduced by 67%. Such dramatic decrease in lattice thermal conductivity with pressure is quite anomalous, since as mentioned earlier generally the thermal conductivity of bulk materials, e.g., diamond, boron nitride, solid argon, would increase under pressure. Moreover, it is worth pointing out that, considering the positive effect of pressure on the electronic property for most thermoelectric materials [48–50], this negative pressure effect on the lattice thermal conductivity could offer an alternative route to decouple the electrical and phononic transport in thermoelectrics in terms of improving their energy conversion performance [51]. Currently, we are continuing the study of other similar thermoelectric systems in this line.

In order to elucidate the reasons for this anomalous pressure-dependent thermal conductivity of HgTe, we examine the phonon mode properties based on the solution of PBTE (Fig. 3). Here different phonon modes are sorted by their frequencies, which is a commonly used method to distinguish different phonon modes in the entire Brillouin zone. Figure 3(a) shows the pressure-dependent specific heat of HgTe at three typical temperatures. At room temperature the specific heat of HgTe at 0 GPa is $1.213 \times 10^6 \text{ J/m}^3 \text{ K}$ ($\sim 48.93 \text{ J/mol K}$), which agrees very well with previous theoretical and experimental data [42,52]. Under the pressure, the specific heat has very little increase with pressure especially for the low temperature (only $\sim 2.7\%$ increase at room temperature). In Fig. 3(b) the average values of group velocity for each phonon branch are plotted. Here, the average value of group velocity is the arithmetic mean, i.e., the sum of all the group velocity divided by the total number of q points in the Brillouin zone. Similar to the variation of specific heat, a slight increase in group velocity is observed in the acoustic phonon modes (LA and TA2) of HgTe under compression, while the group velocities for the optic phonon modes seem unaltered over the entire pressure region. These behaviors are consistent with the observation from the phonon dispersion curves as shown in Fig. 1. Another key factor of the lattice thermal conductivity, phonon lifetime τ , is plotted in Fig. 3(c). It can be clearly seen that the pressure leads to an evident reduction of acoustic phonon lifetime, in particular for TA branches, while the pressure effect on the lifetime of optic phonon modes is minor. These results indicate that the enhancement of acoustic phonon scattering (corresponding to shorter phonon lifetime) is the main reason for the reduced lattice thermal conductivity under pressure, rather than the specific heat and group velocity change [both have slight positive effects on the lattice thermal conductivity, according to Eq. (1)].

The mode specific Grüneisen parameter (γ_λ) [19,34,53] is another way to qualitatively characterize the magnitude of individual three-phonon scattering in a solid material and it can be calculated from the anharmonic IFCs as [19]

$$\gamma_\lambda = -\frac{1}{6\omega_\lambda^2} \sum_k \sum_{l'k'} \sum_{l''k''} \sum_{\alpha\beta\gamma} \left[\Phi_{\alpha\beta\gamma}(0k, l'k', l''k'') \frac{e_{\alpha k}^{\lambda*} e_{\beta k'}^{\lambda'}}{\sqrt{M_k M_{k'}}} \times e^{iqR_{l'}} r_{l''k''\gamma} \right], \quad (2)$$

where $R_{l'}$ is the lattice vector locating in the l' th unit cell; k denotes an atom in this unit cell and the corresponding mass is M_k ; α , β , and γ are Cartesian components; $\Phi_{\alpha\beta\gamma}(0k, l'k', l''k'')$

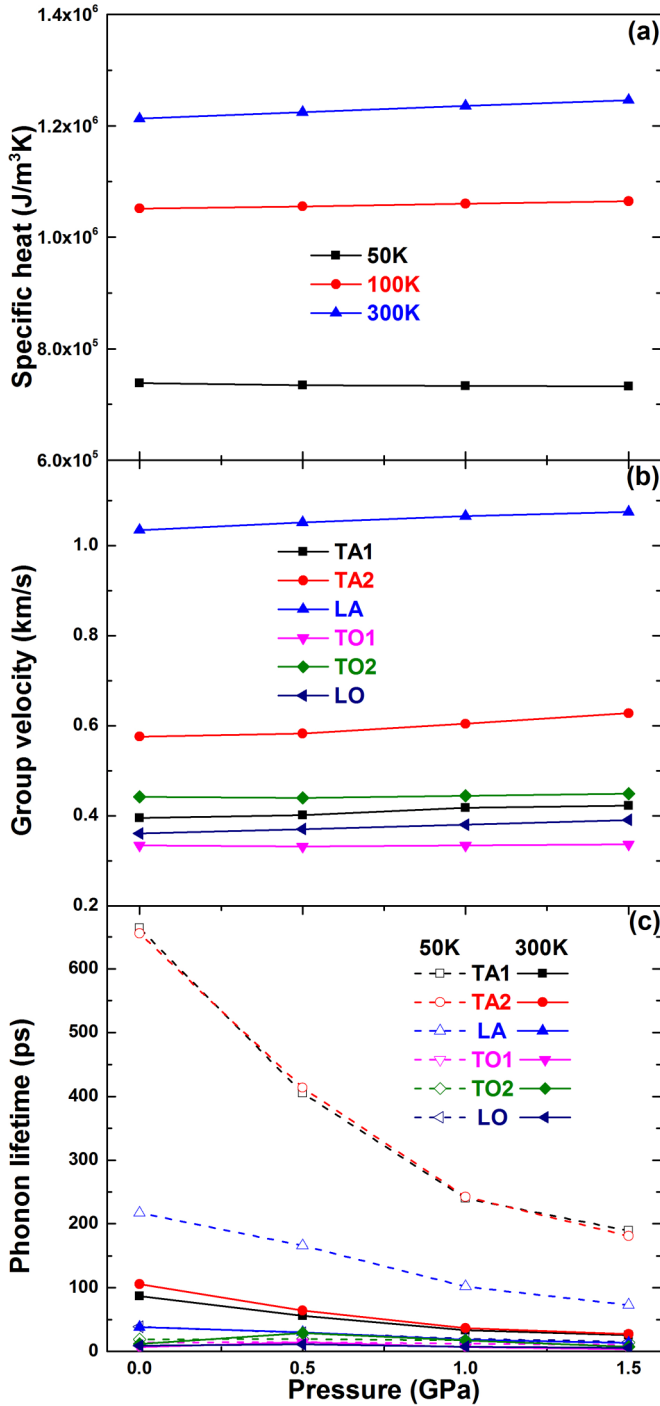


FIG. 3. (Color online) The phonon mode properties, i.e., (a) specific heat, (b) group velocity, and (c) phonon lifetime of HgTe versus pressure.

is the third-order (anharmonic) IFCs; $e_{\alpha k}^{\lambda}$ is the α th component of the phonon eigenvector for atom k in mode λ ; $r_{lk\gamma}$ is the γ th component of the vector locating in the k th lattice atom at the l th unit cell. The Grüneisen parameters can be also calculated by the PHONOPY [44] using the original definition, $\gamma = -d \ln \omega / d \ln V$, where ω and V are phonon frequency and crystal volume [53]. Our calculation shows that the Grüneisen parameters obtained by these two methods are in good agreement with each other (the data are not shown here), indicating

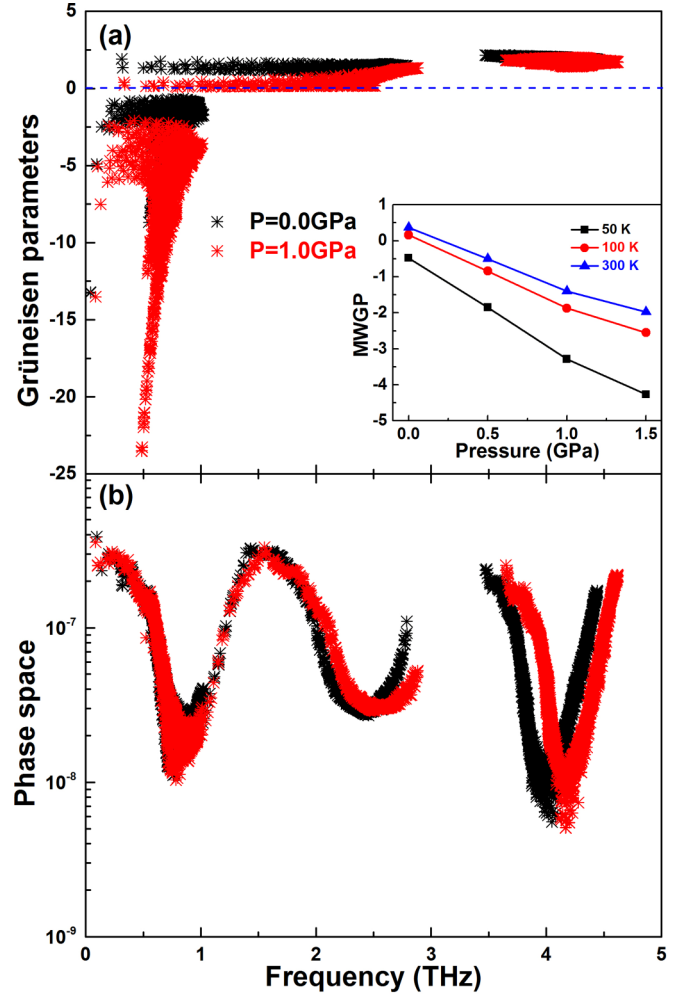


FIG. 4. (Color online) (a) Frequency-dependent mode specific Grüneisen parameter of HgTe at typical pressures. (b) Frequency-dependent three-phonon scattering phase space of HgTe at typical pressure. (a) Inset: The pressure-dependent mode weighted accumulative Grüneisen parameter (MWGP).

that the Grüneisen parameters obtained in our calculation are correct. In Fig. 4(a) the mode specific Grüneisen parameters of HgTe are plotted. From this figure, one can observe notable negative Grüneisen parameters for phonon frequency below 1.2 THz, which corresponds to the TA modes in the phonon spectrum. Under pressure, the negative values of Grüneisen parameters in the low-frequency region continuously move downward (in the negative direction), indicating the magnitude of the absolute value is ascending. From the mode weighted accumulative Grüneisen parameter $\gamma = \sum_{\lambda} C_{\lambda} \gamma_{\lambda} / \sum_{\lambda} C_{\lambda}$, we can see this behavior more clearly [see the inset of Fig. 4(a)]. The calculated cumulative Grüneisen parameter of XTe is also compared with the experimental value in Table I. In Fig. 4(b), three-phonon scattering phase space of HgTe, which could decide the number (space) of phonon scattering processes [55], is also depicted. It can be seen that the pressure effect imposes a weak influence on the phonon scattering space. Based on the qualitative relationship between the phonon lifetime and Grüneisen parameters [53,56], one can conclude that the anharmonic phonon scattering in HgTe is augmented when

TABLE I. Comparison of calculated cumulative Grüneisen parameters (300 K) of XTe and experimental data ([Refs. [53,54]).

Material	γ^{exp}	γ^{cal}
HgTe	0.46	0.37
CdTe	0.52	0.54
ZnTe	0.97	0.81

applying pressure and thus leads to the significant reduction of lattice thermal conductivity.

B. CdTe

Since Cd and Hg belong to the same group in the periodic table, it is intuitive to compare the results between HgTe and CdTe. Analogous to HgTe, we first calculate the phonon dispersion curve and density of state of CdTe as shown in Fig. 5. Our calculated phonon frequencies agree very well with the experimental measurements, which proves the accuracy of our harmonic IFCs. For instance, the calculated frequencies of TO and LO phonon modes at the Γ point are about 4.48 and 5.02 THz, while the experimental data are about 4.20 and 5.08 THz [57]. On the other hand, in contrast to the evident band gap between the acoustic and optic phonon branches in HgTe, there is no band gap between these two types of phonon branches in the spectrum of CdTe. This disappearance of phonon band gap is mainly attributed to the smaller mass ratio between Cd and Te atoms. Similar phenomena have also been reported in the literature [26,58]. With applied pressure, it can be seen that pressure barely alters transverse acoustic phonons (again except for slightly softening around the X and K points), but shifts the longitudinal acoustic phonons and the optic phonons to higher frequencies. This behavior of phonon branches is similar to that observed in HgTe.

Figure 6 shows the pressure-dependent thermal conductivity for the case of CdTe at three typical temperatures. The calculated thermal conductivity of CdTe at room temperature is about 13.22 W/mK, in contrast to the experimental value of about 7.50 W/mK [59]. A striking result in Fig. 6 is the different response of thermal conductivity to pressure at different temperatures. At low temperature (50 K), the pressure has a negative effect on the thermal conductivity of CdTe, similar to that in HgTe; i.e., the thermal conductivity decreases with increase of pressure. However, at high temperatures (100

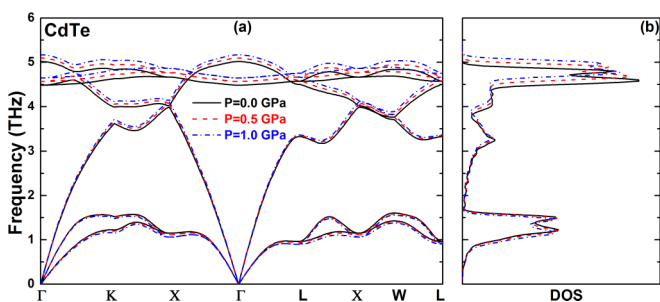


FIG. 5. (Color online) (a) The phonon spectra of CdTe under different pressures and (b) corresponding phonon density of state (DOS).

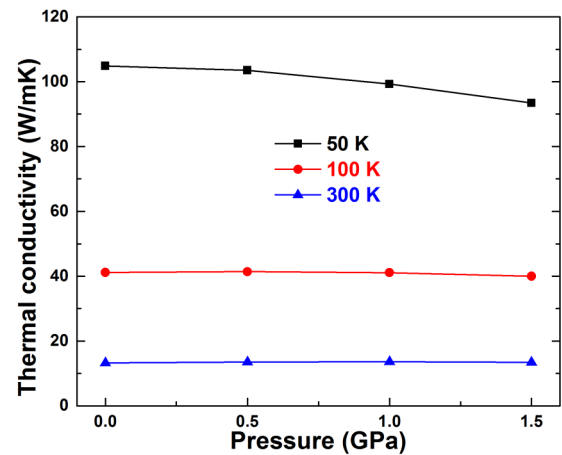


FIG. 6. (Color online) The lattice thermal conductivity of CdTe as a function of pressure at three typical temperatures.

and 300 K), the thermal conductivity remains as a constant over the pressure range from 0 to 1.5 GPa.

In Fig. 7, the phonon mode properties of CdTe are presented to understand the different response of thermal conductivity to pressure. The room temperature specific heat of CdTe at 0 GPa is 1.005×10^6 J/m³K (~ 48.57 J/mol K), which agrees very well with the previous experimental value of 50.05 J/mol K [60]. When pressure is applied, we can see from Fig. 7(a) that the specific heat of CdTe has a slight increase with pressure. As shown in Fig. 7(b), similar variation can also be observed for the average phonon group velocity of CdTe, especially for the LA phonon modes. Meanwhile, the average group velocity of CdTe is larger than that of HgTe shown in Fig. 3(b), which originates from the larger slope of phonon branches versus the phonon wave vector and higher cutoff frequency in the phonon spectrum, a nature of stronger interatomic interaction between Cd and Te atoms. Figure 7(c) gives the pressure-dependent mean phonon lifetime of CdTe for each phonon branch. Unlike the significant reduction in the lifetime of dominated phonons (acoustic phonons) in HgTe, there only exists a slight decrease in the phonon lifetime of TA modes in CdTe with pressure at low temperature (50 K). As temperature increases, this decrease of phonon lifetime gradually disappears. Combining the variation of specific heat, group velocity, and phonon lifetime with pressure, we know that at low temperature the considerable drop in the phonon lifetime overwhelms the incremental change in the specific heat and group velocity, while at higher temperatures the drop in the phonon lifetime compensates the slight augmentation in the specific heat and group velocity. Therefore, according to Eq. (1), the lattice thermal conductivity of CdTe has little dropdown with pressure at low temperature and is almost pressure independent at high temperatures (Fig. 6).

In order to further understand the phonon anharmonicity in CdTe, in Figs. 8(a) and 8(b) we plot the mode specific Grüneisen parameter γ_λ and three-phonon phase space with different pressures. The Grüneisen parameters of CdTe at some high symmetric points are also compared with previous theoretical data [61]. It can be seen that there also exist notable negative Grüneisen parameters in the low-frequency region, which originate from the TA phonon modes. However, the

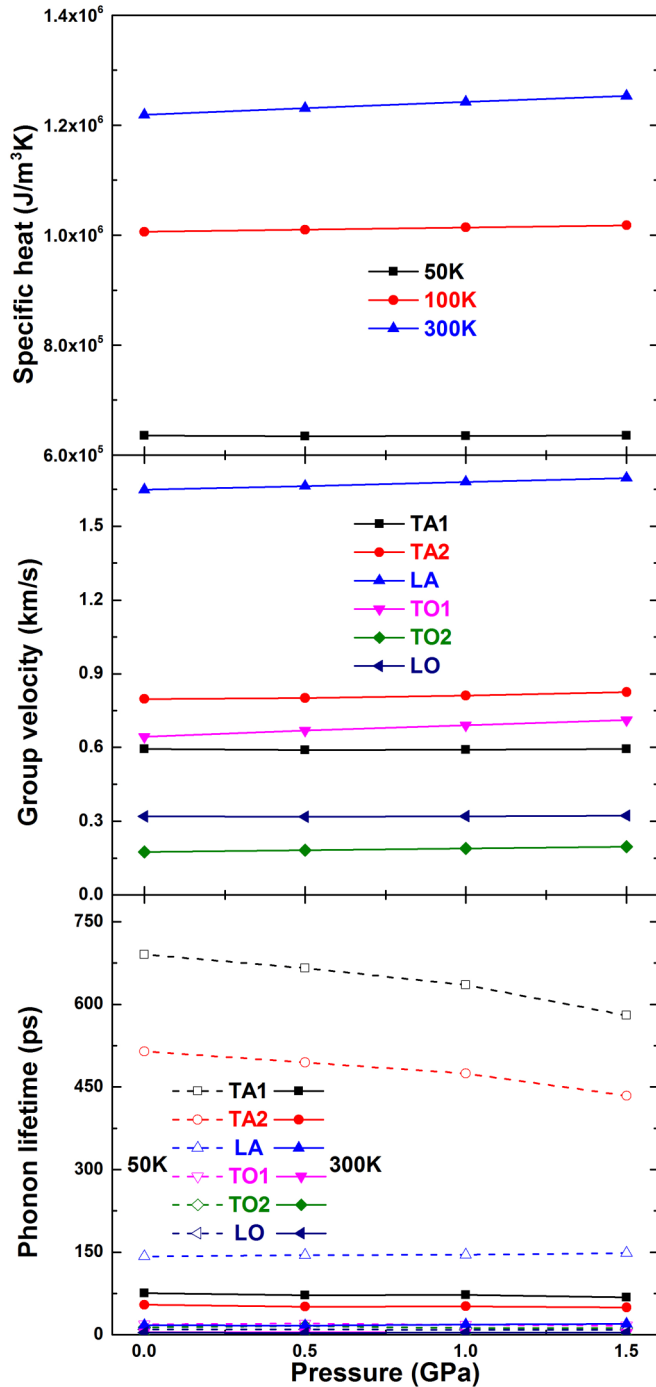


FIG. 7. (Color online) The phonon mode properties, i.e., (a) specific heat, (b) group velocity, and (c) phonon lifetime of CdTe versus pressure.

magnitude of these negative Grüneisen parameters in CdTe is far smaller than that in HgTe shown in Fig. 4(a). Under compression, the change in the Grüneisen parameters and three-phonon phase space of CdTe is also indistinctive. There only exists a slight decrease in the negative part as shown in the inset of Fig. 8(a). At low temperature (50 K), only low-frequency phonon modes contribute to the thermal transport. Therefore, the slight downward move of the low-frequency phonon modes with negative Grüneisen parameters, i.e., the

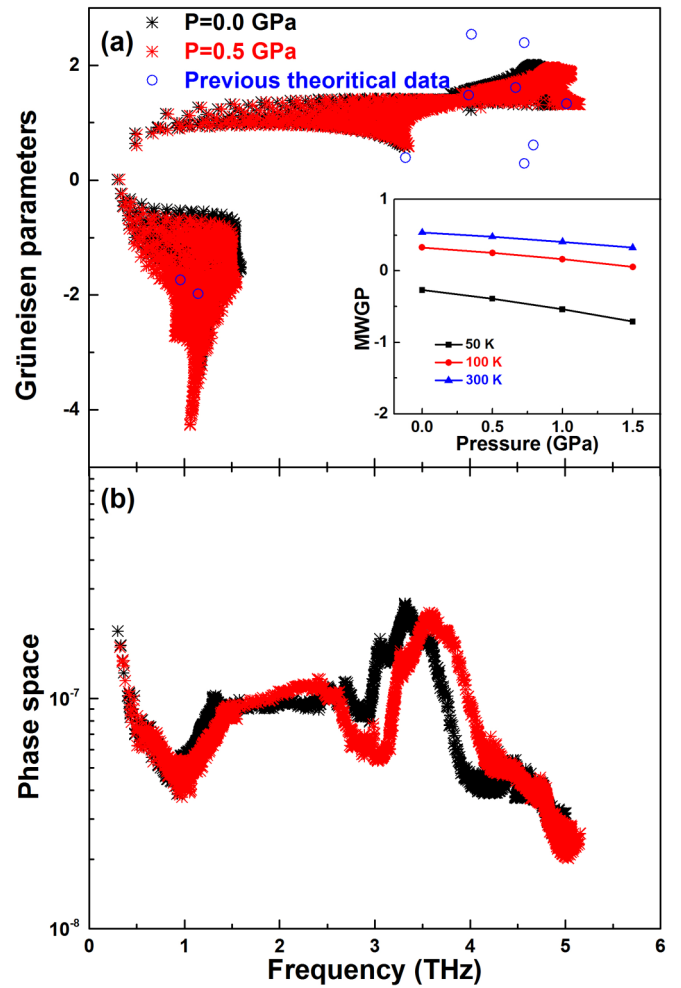


FIG. 8. (Color online) (a) Frequency-dependent mode specific Grüneisen parameter of CdTe at typical pressures. Comparison of the Grüneisen parameters at some high symmetric points between our calculation and previous theoretical data ([Ref. [61]]) is also provided. (b) Frequency-dependent three-phonon scattering phase space of CdTe at typical pressure. (a) Inset: The pressure-dependent mode weighted accumulative Grüneisen parameter (MWGP).

increase in the absolute value, will enhance the intrinsic phonon-phonon scattering at low temperature and gives rise to the slight decrease of the lattice thermal conductivity, as shown in Fig. 6. As the temperature increases (100 and 300 K), however, the high-frequency phonon modes start to contribute to thermal conductivity as well, and the weak enhancement of the Grüneisen parameters in the low-frequency region could be attenuated; i.e., the positive value of the Grüneisen parameters is decreased (see the inset of Fig. 8). Consequently, the thermal conductivity of CdTe is independent of pressure at 100 and 300 K.

C. ZnTe

As a comparison with HgTe and CdTe, we finally calculate the pressure effect on the thermal transport in ZnTe. The phonon spectra of ZnTe with different pressures are plotted in Fig. 9. The calculated phonon frequencies also match very well with the experiments. For example, the calculated frequencies

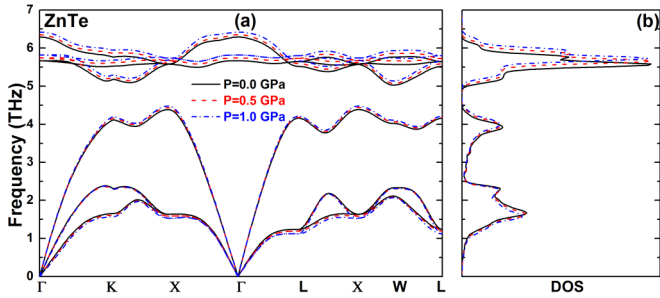


FIG. 9. (Color online) (a) The phonon spectra of ZnTe under different pressures and (b) corresponding phonon density of state (DOS).

of TO and LO phonon modes at the Γ point are about 5.66 and 6.29 THz, respectively, as compared with the experimental value of about 5.30 and 6.20 THz [62]. Similar to HgTe, there also exists an obvious band gap between the acoustic and optic phonon branches owing to the large mass ratio between the Zn and Te atoms. Due to the stronger bonding energy in ZnTe, the cutoff frequency of ZnTe is higher than that in HgTe and CdTe, which foreshadows the larger group velocity in ZnTe (see below in Fig. 11). Upon compression, the analogous phenomena found in HgTe and CdTe can be observed in ZnTe as well.

As for the pressure effect on the thermal conductivity of ZnTe, we can see from Fig. 10 that, at all temperatures considered in this work, the thermal conductivity of ZnTe is independent of pressure. This trend is consistent with that for bulk silicon [17], while in contrast to that for HgTe and CdTe at low temperature, where the thermal conductivity largely decreases under compression. In order to interpret the pressure-independent thermal transport property of ZnTe at the phonon mode level, in Figs. 11(a)–11(c) we plot the average specific heat, group velocity, and phonon lifetime as a function of pressure. From these figures, it can be seen that not only the harmonic effect (specific heat and group velocity) but also the anharmonic effect (phonon lifetime) in ZnTe hardly changes under compression, which obviously explains the pressure dependence of thermal conductivity.

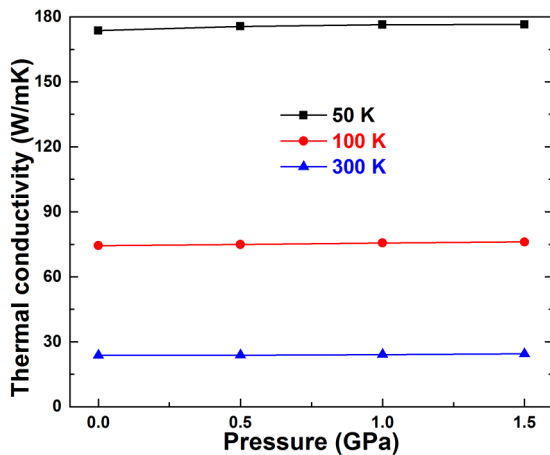


FIG. 10. (Color online) The lattice thermal conductivity of ZnTe as a function of pressure at three typical temperatures.

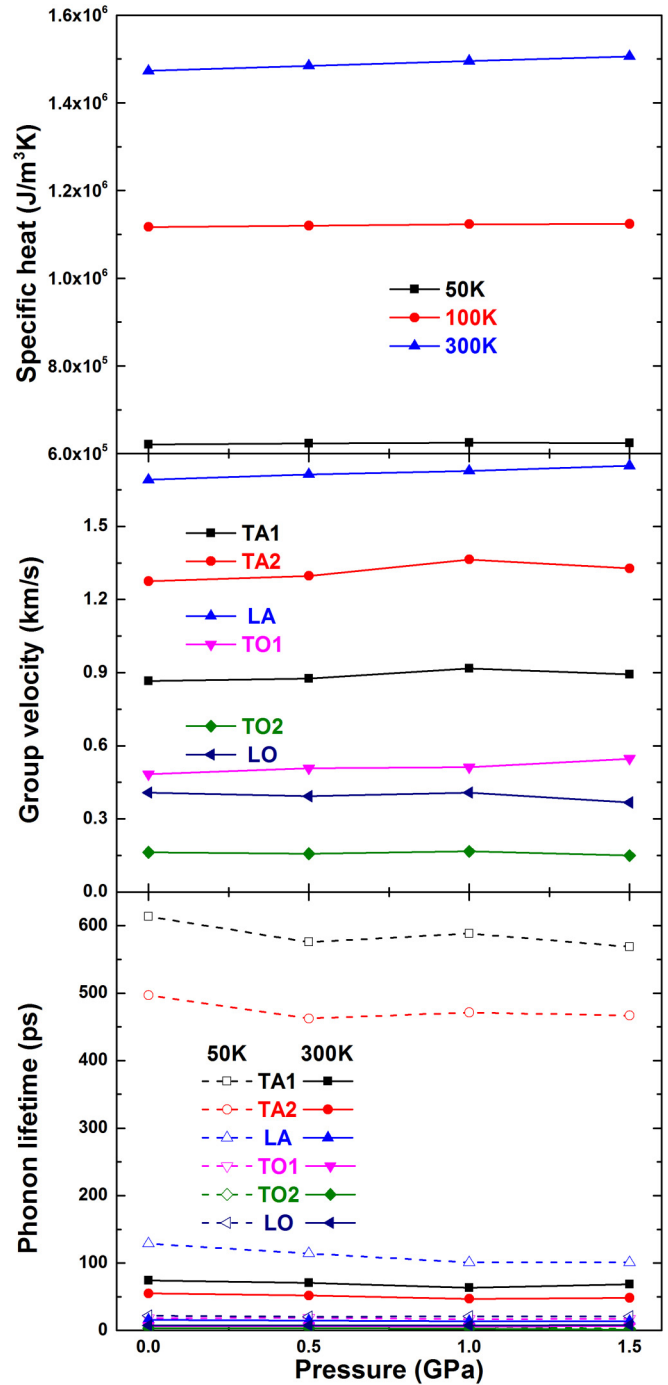


FIG. 11. (Color online) The phonon mode properties, i.e., (a) specific heat, (b) group velocity, and (c) phonon lifetime of ZnTe versus pressure.

Figures 12(a) and 12(b) give the mode specific Grüneisen parameters and three-phonon phase space of ZnTe. The Grüneisen parameters of ZnTe at some high symmetric points are also compared with experimental data [63]. The magnitude of the negative Grüneisen parameters γ_λ that originated from the low-frequency TA phonon modes is obviously lower than that in HgTe and CdTe. Meanwhile, there also exist a certain amount of positive Grüneisen parameters (originated from the LA phonon modes) in the low-frequency region, which

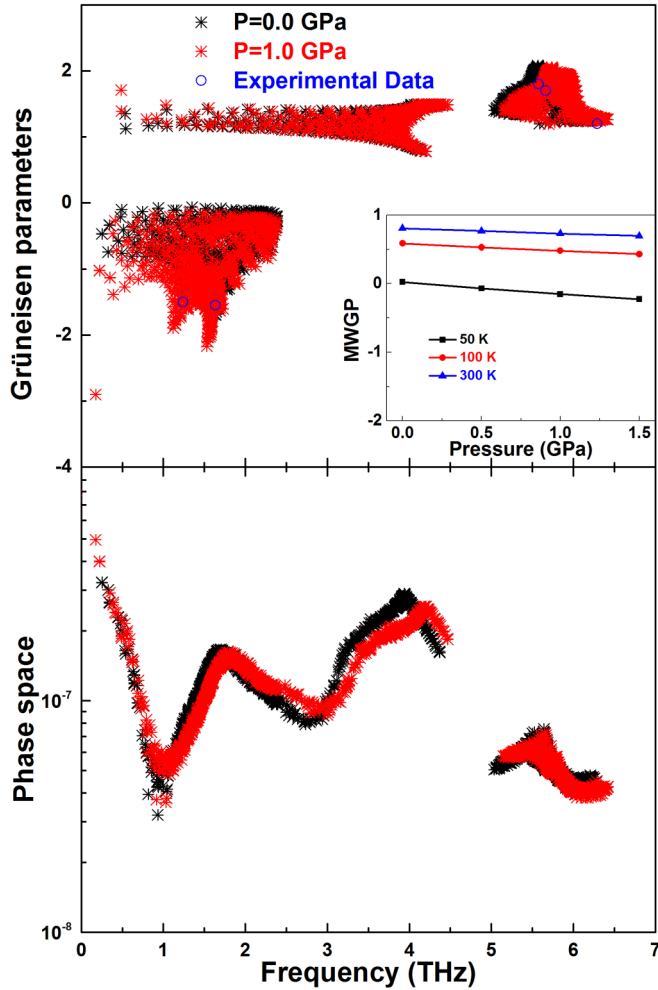


FIG. 12. (Color online) (a) Frequency-dependent mode specific Grüneisen parameter of ZnTe at typical pressures. Comparison of the Grüneisen parameters at some high symmetric points between our calculation and experimental data ([Ref. [63]]) is also provided. (b) Frequency-dependent three-phonon scattering phase space of HgTe at typical pressure. (a) Inset: The pressure-dependent mode weighted accumulative Grüneisen parameter (MWGP).

weakens the negative part of the Grüneisen parameters. When pressure is applied, the variation of the Grüneisen parameters (see the inset of Fig. 12) and three-phonon phase space is quite small, indicating that the pressure has a weak influence on the phonon anharmonicity in ZnTe. Therefore, the lattice thermal conductivity of ZnTe remains as a constant with increase of pressure.

IV. FURTHER ANALYSIS OF UNDERLYING MECHANISM OF STRAINED PHONONS

From the results presented above, a qualitative conclusion can be drawn that the pressure mainly possesses two competing effects on the lattice thermal conductivity of XTe [Eq. (1)]. On the one hand, the pressure will improve the specific heat and the group velocity (especially the LA and optic phonon modes), which is the “positive” effect on the phonon transport. On the other hand, the pressure will enhance the phonon

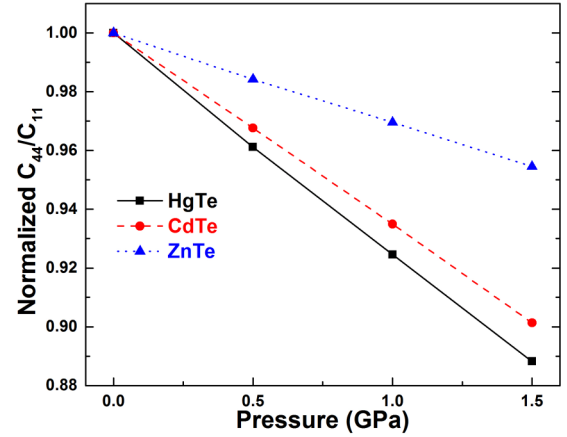


FIG. 13. (Color online) The normalized C_{44}/C_{11} of HgTe, CdTe, and ZnTe as a function of pressure.

anharmonicity of TA phonon modes as well, which represents the “negative” effect on the thermal conductivity. Generally speaking, the positive effect of pressure is a universal behavior for a rather large amount of bulk materials. Therefore, the variation of thermal conductivity with pressure is mainly determined by the magnitude of the negative effect; i.e., when the phonon anharmonicity of TA modes overwhelms the “positive” effect, the lattice thermal conductivity should decrease with pressure. In the following, we present three different physical parameters to characterize the phonon anharmonicity, which might be helpful in revealing and understanding the underlying mechanism more clearly.

A. The relationship between elastic constants and phonon anharmonicity

It is well known that the physical properties of phonon modes also correlate with the elastic constants of a material [64]. In order to analyze the relationship between the elastic constants and the pressure dependence of lattice thermal conductivity, in Fig. 13 we plot the normalized C_{44}/C_{11} as a function of pressure, where C_{11} and C_{44} are the first and the fourth elements on the diagonal of the elastic constant tensor. The C_{44}/C_{11} is normalized by the value at zero pressure. It can be seen that the normalized C_{44}/C_{11} of XTe decreases evidently as the pressure increases. Moreover, the decreasing slope of the normalized C_{44}/C_{11} with respect to pressure is quite different and the sequence is as follows: HgTe > CdTe > ZnTe, which is consistent with the magnitude of the negative slope of the lattice thermal conductivity with respect to pressure. Since C_{44} can qualitatively determine the phonon frequency of TA modes [65], the decrease of the normalized C_{44}/C_{11} shown in Fig. 13 suggests that the frequency of TA phonon modes will decrease under pressure. According to the direct definition of the Grüneisen parameter, $\gamma = -d \ln \omega / d \ln V$, if the frequency of TA phonon modes decreases with pressure, then the negative Grüneisen parameters could be induced in the TA phonon modes and the magnitude is determined by the decreasing slope of the normalized C_{44}/C_{11} . That is to say, among the three materials studied, the HgTe possesses the strongest phonon anharmonicity, while ZnTe holds the weakest

phonon anharmonicity with pressure. Owing to the large decreasing slope of normalized C_{44}/C_{11} (i.e., enhancement of phonon anharmonicity) in HgTe, the improvement of specific heat and group velocity cannot compete with the negative aspect induced by the phonon anharmonicity. Therefore, the thermal conductivity of HgTe decreases monotonically with pressure. As for ZnTe, the pressure effect on the phonon anharmonicity is weak and the positive effect of pressure could neutralize this negative part, which gives rise to the pressure independence of thermal conductivity. For CdTe, the negative effects dominate the thermal transport only at low temperatures (the TA phonon modes play a critical role in the thermal conductivity). Therefore, the thermal conductivity of CdTe only slightly decreases at low temperature while it remains as a constant at high temperature. Based on this analysis, the slope of the normalized C_{44}/C_{11} can be used to quantify the magnitude of the negative effect (phonon anharmonicity) of pressure, e.g., XTe in our calculation, bulk Si, and diamond. However, it should be note here that whether this qualitative conclusion can be extended to other new materials needs further investigations in the future.

B. The relationship between the coefficient of thermal expansion and thermal conductivity

From the theory of thermodynamics, the Grüneisen parameters can also be used to quantify the volumetric coefficient of thermal expansion (CTE) α_V [66] by

$$\alpha_V = \frac{1}{B} \sum_{\lambda} C_{\lambda} \gamma_{\lambda}, \quad (3)$$

where B is the bulk modulus. In this work, we treat the bulk modulus as a temperature-independent parameter for simplification. From this aspect of analysis one can speculate that there should exist a relationship between the thermal conductivity and coefficient of thermal expansion. In order to demonstrate our conjecture, in Fig. 14 we present the volumetric coefficient of thermal expansion of HgTe, CdTe, and ZnTe at different pressures. From Fig. 14(a) one can notice that over a wide temperature range (0–75 K) there are obvious negative coefficients of thermal expansion in HgTe, due to the large intrinsic negative Grüneisen parameters in the low-frequency region (Fig. 4). Under compression, the magnitude of the negative thermal expansion of HgTe becomes larger and the corresponding temperature range is extended to the entire temperature considered here. Similar results have also been reported in a previous experimental study [67], where negative thermal expansion of HgTe under pressure of 1.2 GPa can be found at a temperature as high as 300 K. As for CdTe shown in Fig. 14(b), the volumetric coefficient of thermal expansion also possesses a small negative range (<60 K) and it moves downward with pressure increasing as well. However, the coefficient of thermal expansion of CdTe at high temperature (>60 K) increases to positive at 0 GPa and the temperature corresponding to the negative-positive transition of CTE moves rightward (up to 100 K) under high pressure. For ZnTe [Fig. 14(c)], it can be seen that the variation of coefficient of thermal expansion with pressure is not appreciable as compared to that in HgTe and CdTe. The magnitude of the negative thermal expansion of

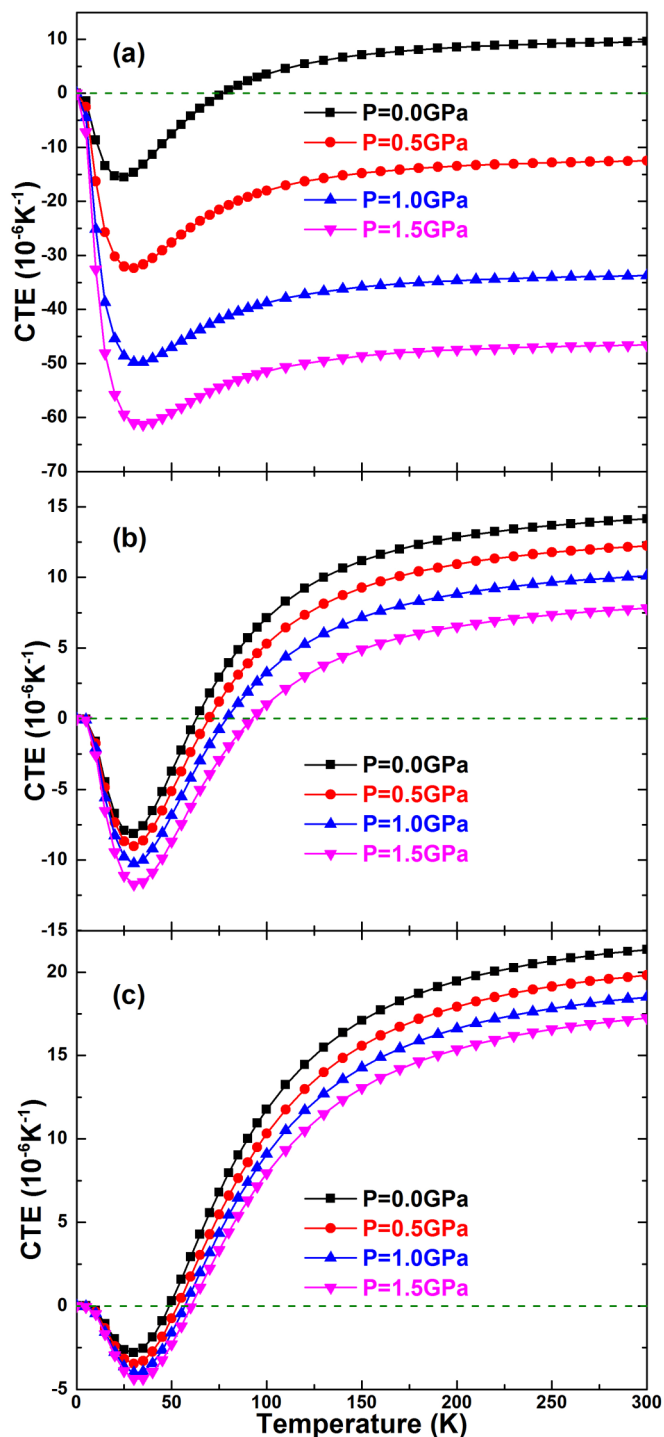


FIG. 14. (Color online) The volumetric coefficient of thermal expansion of (a) HgTe, (b) CdTe, and (c) ZnTe as a function of temperature at typical pressure.

ZnTe is much smaller than that of HgTe and CdTe and the negative temperature range becomes much narrower (<60 K) for all pressures considered. The CTE always holds positive in a wide range of temperature (>60 K). Based on the results presented above, one can obtain qualitative conclusions about the relationship between the coefficient of thermal expansion and the lattice thermal conductivity: (1) the negative pressure effect on the thermal conductivity is always accompanied with

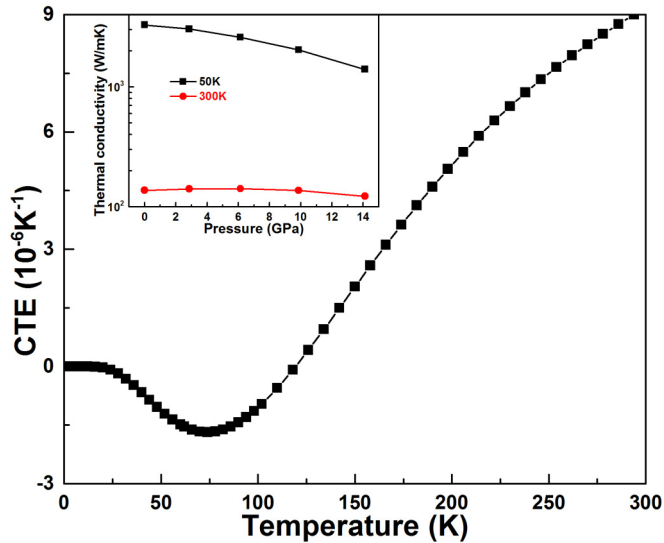


FIG. 15. (Color online) The volumetric coefficient of thermal expansion of bulk silicon. Inset: The lattice thermal conductivity of bulk silicon as a function of pressure at 50 and 300 K.

large negative coefficient of thermal expansion; (2) the notable variation of the coefficient of thermal expansion to negative is more likely to result in considerable reduction of lattice thermal conductivity upon applying pressure.

In order to further demonstrate our speculation on the relationship between negative CTE and negative pressure-dependent thermal conductivity, in Fig. 15 we calculate the corresponding thermal transport properties of bulk silicon with similar atomic structure to XTe . It can be clearly seen that there exists a negative coefficient of thermal expansion region (<125 K) in the bulk silicon, which agrees very well with previous theoretical and experimental measured results [68,69]. Accordingly, based on our speculation, the negative coefficient of thermal expansion of bulk silicon foreshows the negative pressure dependence of thermal conductivity in this temperature region. From the inset of Fig. 15, we can find that the calculated thermal conductivity of silicon matches our speculation very well. The lattice thermal conductivity of silicon decreases largely with pressure at 50 K (in the negative coefficient of the thermal expansion region), while it remains almost as a constant at room temperature. The latter is consistent with previous theoretical and experimental studies [17,25]. The diamond, whose thermal expansion is always positive in the entire temperature region, is also tested. We find that the thermal conductivity of diamond continuously increases with pressure for all temperatures considered (50–300 K; the results are not shown for brevity). These extended cases further prove the reliability of our speculation on the relationship between CTE and thermal conductivity.

C. Correlation between the nature of interatomic interaction and pressure dependence of lattice thermal conductivity

Finally, in order to correlate the diverse pressure-dependent thermal transport phenomena with interatomic interaction, in Fig. 16 we calculate the deformation charge density (DCD) distribution of the ground state HgTe, CdTe, and ZnTe. From

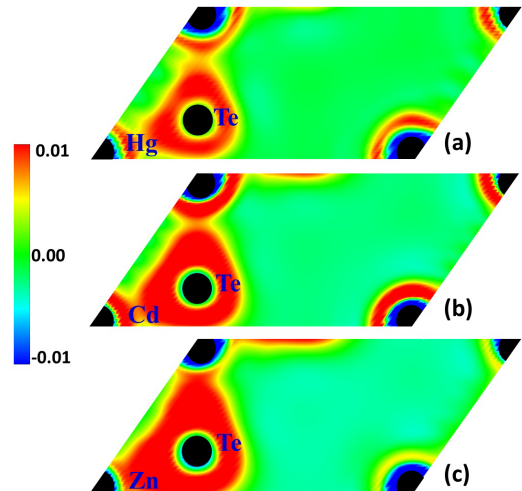


FIG. 16. (Color online) Deformation charge density in units of $e/\text{\AA}^3$ projected onto the $(1\bar{1}0)$ plane of (a) HgTe, (b) CdTe, and (c) ZnTe at ground state. Each black dot represents an atom and is labeled in blue.

the distribution of DCD, it can be clearly seen that for HgTe the electrons are mainly transferred to the Te atoms as shown in Fig. 16(a), indicating an ionic bonding. In contrast, for CdTe and ZnTe [see Figs. 16(b) and 16(c), respectively], the corresponding distribution of DCD is totally different, where the electrons are gradually transferred to the region between the Cd (Zn) and Te atoms. This different feature of DCD distribution suggests that the interatomic bonding becomes more covalent in CdTe and ZnTe as compared to that in HgTe. That is to say, the interatomic bonds in HgTe are partially ionic, while the bonds in CdTe and ZnTe are partially covalent. On the one hand, we know that the covalent bond possesses strong directivity and thus the atom slide hardly occurs, which leads to the indistinctive negative Grüneisen parameters, as found in other materials (e.g., Si and diamond [70–72]), and the positive volumetric coefficient of thermal expansion. On the other hand, the atoms with ionic bonding can slide with each other easily, owing to the nondirectivity in the ionic bonds. In this case, remarkable negative Grüneisen parameters in the low-frequency acoustic phonon modes and the negative volumetric coefficient of thermal expansion could be observed. Similar phenomena have also been found in other systems, e.g., CuCl [73] and AgI [74]. Consequently, the materials (HgTe) with partially ionic bonding always have a large magnitude of negative Grüneisen parameters (inducing strong phonon anharmonicity, Fig. 4) and low thermal conductivity as compared to those (ZnTe) with partially covalent bonding [75]. Upon compression, the slide motion of atoms in HgTe is enhanced and induces stronger anharmonic scattering, which gives rise to the negative coefficient of thermal expansion and decreased thermal conductivity. For ZnTe, the intrinsic slide motion of atoms (negative Grüneisen parameters, Fig. 12) is relatively weak and insensitive to pressure, thus leading to the pressure-independent coefficient of thermal expansion and thermal conductivity. As for the middle case of CdTe, the intension of atom slide motion falls somewhere in between HgTe and ZnTe. Accordingly, the thermal conductivity decreases with pressure at low temperature, where the negative

Grüneisen parameters are evident, and remains as a constant at high temperature owing to the neutralization of the negative Grüneisen parameters of TA modes by the positive Grüneisen parameters of LA and optic modes (Fig. 8).

V. SUMMARY AND CONCLUSION

To summarize, we have presented a systematic study and comparison of the pressure effect on the lattice thermal conductivity of bulk telluride systems $X\text{Te}$ ($X = \text{Hg}, \text{Cd}, \text{Zn}$) at different temperatures by solving the Peierls-Boltzmann transport equation with interatomic force constants calculated from first principles. Our results show that the thermal conductivity of $X\text{Te}$ presents totally different pressure dependence. The thermal conductivity of HgTe decreases largely with pressure at all temperatures and the degree of decreasing ascends when the temperature gets lower. For CdTe , the thermal conductivity only slightly decreases with pressure at low temperature (50 K), while it remains constant at high temperatures (100 and 300 K). As for ZnTe , however, the thermal conductivity is independent of pressure for all temperatures considered. By comparing the key factors of the lattice thermal conductivity at the phonon mode level, we find that the different response of the lattice thermal conductivity to the external pressure mainly depends on the competition between the enhancement of group velocity of LA and optic modes (positive effect on thermal conductivity) and the reduction of phonon relaxation time of TA modes induced by the phonon anharmonicity (negative effect). Further analysis reveals that the magnitude and variation of the intrinsic negative Grüneisen parameters of the transverse acoustic modes are the key and governing parameters for determining the negative pressure-dependent thermal conductivity, when they overwhelm the positive effect of the enhancement of group velocity. Finally, the analysis of the electronic density distribution establishes the correlation between the diverse thermal transport phenomena and the nature of the interatomic interactions. The material with ionic bonding is more likely to possess large negative Grüneisen parameters and negative coefficient of thermal expansion in a very wide temperature range (sometimes can even persist above room temperature). As a result, the negative pressure effect on the lattice thermal conductivity generally appears in this type of material. In contrast, when the material has covalent bonding, the negative Grüneisen parameters and negative coefficient of thermal expansion can only occur at very low temperatures. As temperature increases, both the average Grüneisen parameter and the coefficient of thermal expansion transits from negative to positive, and thus the effect of pressure on the lattice thermal conductivity is positive as well. Simulations of bulk silicon further underpin our conclusion.

It should be noted here that our speculation about the thermal expansion and thermal conductivity has been demonstrated not only for $X\text{Te}$ in our calculation, but also for bulk Si. Thus in our opinion this speculation can also be extended to other materials with dominant negative Grüneisen parameters or a global negative thermal expansion coefficient. For example, the negative pressure dependence of thermal conductivity can also be found in Si clathrate frameworks. For Si-VII ($I\bar{m}-3m$) structure the thermal conductivity drops by 43% when the volume is compressed by 3%, as revealed by our

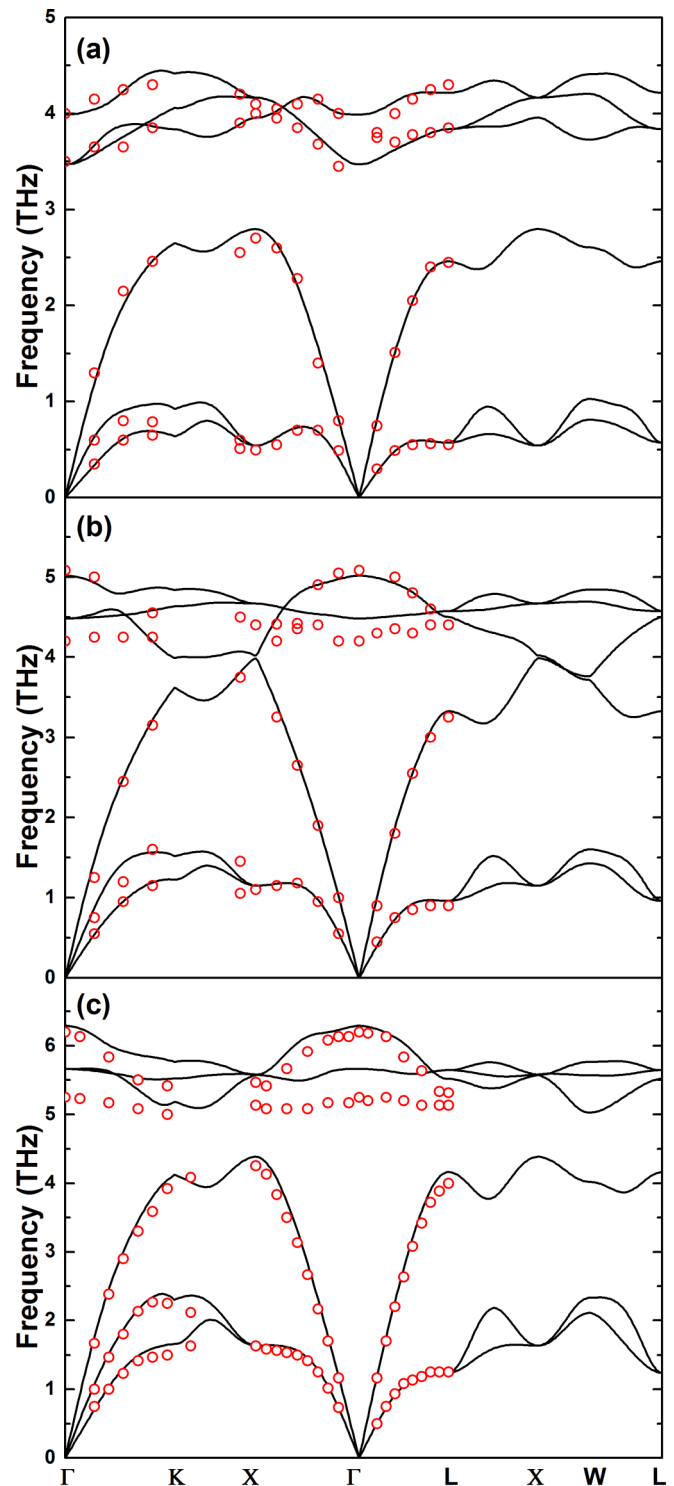


FIG. 17. (Color online) Comparison of the phonon dispersion curves of (a) HgTe , (b) CdTe , and (c) $X\text{Te}$ between our calculation and experimental data in different symmetry directions of the Brillouin zone. Open circles are the neutron-scattering data taken from HgTe , Ref. [42]; CdTe , Ref. [57]; ZnTe , Ref. [62].

recent *ab initio* calculations (results not shown here for brevity). We also found the same negative pressure-dependent lattice thermal conductivity for other binary thermoelectric materials and even ternary materials recently. As for the theoretical

explanation of mass ratios for negative pressure dependence of thermal conductivity [26], it indeed makes a good prediction on some special binary compound materials. However, this explanation cannot be directly applied to the present systems, in particular for the bulk Si and pure Si clathrates, since they are composed of a single element, not compounds.

As for the fundamental significance of this paper to the microscale/nanoscale heat transfer and also the broad materials science community, we would like to point out that the motivation of this work originates from enhancing the energy conversion performance of thermoelectric materials, where electronic and phononic transport property is inherently and strongly coupled, which significantly hinders the large improvements of the ZT coefficient $ZT = S^2\sigma T/\kappa$, where κ ($\kappa = \kappa_e + \kappa_p$) is the thermal conductivity composed of the contributions from electrons (κ_e) and phonons (κ_p). Our paper reveals that, by using negative thermal expansion materials under pressure, the lattice thermal conductivity can be largely reduced, and at the same time the electronic transport could be maintained or even enhanced under pressure. In the present work we do not calculate the electronic transport properties with pressure. However, previous studies have shown the positive effect of pressure on the electronic properties (electrical conductivity, Seebeck coefficient, or thermopower) of several materials, such as PbTe, Bi-Cu-Se-O, and other thermoelectric materials [48–50]. Therefore, we expect that a similar effect could also be found in other systems and it is worth investigating the corresponding pressure effect on the lattice thermal conductivity.

Simultaneously searching thermoelectric materials with positive pressure effect on the thermopower is underway currently. Our findings provide physical insights into the effect of pressure on the phonon transport of bulk materials at different temperatures and offer an alternative route to effectively decouple the electrical and phononic transport in thermoelectrics in terms of improving their energy conversion performance.

ACKNOWLEDGMENTS

T.O. thanks Dr. Jin Li and Chaoyu He (Xiangtan University) for their helpful discussions. Simulations were performed with computing resources granted by the Jülich Aachen Research Alliance-High Performance Computing (JARA-HPC) from RWTH Aachen University under Project No. jara0132. This work is partly supported by the National Natural Science Foundation of China (Grant No. 11304262), the Hunan Provincial Natural Science Foundation of China (Grant No. 14JJ3074), and the Scientific Research Fund of Hunan Provincial Education Department (Grant No. 13C927).

APPENDIX

In Fig. 17 we compare the phonon dispersion of XTe between our *ab initio* calculation and experimental measurements. The results show that our calculation is in good agreement with experiments.

-
- [1] M. Hu, K. P. Giapis, J. V. Goicochea, X. Zhang, and D. Poulikakos, *Nano Lett.* **11**, 618 (2011).
 - [2] M. Hu, J. V. Goicochea, B. Michel, and D. Poulikakos, *Nano Lett.* **10**, 279 (2010).
 - [3] N. P. Padture, M. Gell, and E. H. Jordan, *Science* **296**, 280 (2002).
 - [4] H. Bao, C. Shao, S. Luo, and M. Hu, *J. Appl. Phys.* **115**, 053524 (2014).
 - [5] V. Samvedi and V. Tomara, *J. Appl. Phys.* **105**, 013541 (2009).
 - [6] C. W. Padgett and D. W. Brenner, *Nano Lett.* **4**, 1051 (2004).
 - [7] D. Donadio and G. Galli, *Phys. Rev. Lett.* **99**, 255502 (2007).
 - [8] W. Li, H. Sevinçli, G. Cuniberti, and S. Roche, *Phys. Rev. B* **82**, 041410(R) (2010).
 - [9] J. H. Seol, I. Jo, A. L. Moore, L. Lindsay, Z. H. Aitken, M. T. Pettes, X. Li, Z. Yao, R. Huang, D. A. Broido, N. Mingo, R. S. Ruoff, and L. Shi, *Science* **328**, 213 (2010).
 - [10] S. Lee, K. Esfarjani, J. Mendoza, M. S. Dresselhaus, and G. Chen, *Phys. Rev. B* **89**, 085206 (2014).
 - [11] E. S. Landry, M. I. Hussein, and A. J. H. McGaughey, *Phys. Rev. B* **77**, 184302 (2008).
 - [12] S. Y. Xiong, Y. A. Kosevich, K. Sääskilähti, Y. X. Ni, and S. Volz, *Phys. Rev. B* **90**, 195439 (2014).
 - [13] X. L. Zhang, H. Bao, and M. Hu, *Nanoscale* **7**, 6014 (2015).
 - [14] R. G. Ross, P. Andersson, B. Sundqvist, and G. Backstrom, *Rep. Prog. Phys.* **47**, 1347 (1984).
 - [15] A. F. Goncharov, M. Wong, D. A. Dalton, J. G. O. Ojwang, V. V. Struzhkin, Z. Konôpková, and P. Lazor, *J. Appl. Phys.* **111**, 112609 (2012).
 - [16] M. Pozzo, C. Davies, D. Gubbins, and D. Alfè, *Nature (London)* **485**, 355 (2012).
 - [17] K. D. Parrish, A. Jain, J. M. Larkin, W. A. Saidi, and A. J. H. McGaughey, *Phys. Rev. B* **90**, 235201 (2014).
 - [18] A. Chernatynskiy and S. R. Phillpot, *J. Appl. Phys.* **114**, 064902 (2012).
 - [19] D. A. Broido, L. Lindsay, and A. Ward, *Phys. Rev. B* **86**, 115203 (2012).
 - [20] X. Li, K. Maute, M. L. Dunn, and R. Yang, *Phys. Rev. B* **81**, 245318 (2010).
 - [21] S. Mukhopadhyay and D. A. Stewart, *Phys. Rev. Lett.* **113**, 025901 (2014).
 - [22] A. A. Abramson, C.-L. Tien, and A. Majumdar, *J. Heat Transfer* **124**, 963 (2002).
 - [23] J. Chen, J. H. Walther, and P. Koumoutsakos, *Nano Lett.* **14**, 819 (2014).
 - [24] T. Ouyang, X. L. Zhang, and M. Hu, *Nanotechnology* **26**, 025702 (2015).
 - [25] G. T. Hohensee, M. R. Fellingner, D. R. Trinkle, and D. G. Cahill, *Phys. Rev. B* **91**, 205104 (2015).
 - [26] L. Lindsay, D. A. Broido, J. Carrete, N. Mingo, and T. L. Reinecke, *Phys. Rev. B* **91**, 121202 (2015).
 - [27] F. A. Devillanova and W. W. D. Mont, *Handbook of Chalcogen Chemistry: New Perspectives in Sulfur, Selenium and Tellurium* (Royal Society of Chemistry, Cambridge, 2013).
 - [28] M. Côté, O. Zakharov, A. Rubio, and M. L. Cohen, *Phys. Rev. B* **55**, 13025 (1997).

- [29] R. J. Nelmes, M. I. McMahon, N. G. Wright, and D. R. Allan, *Phys. Rev. Lett.* **73**, 1805 (1994).
- [30] M. I. McMahon, R. J. Nelmes, N. G. Wright, and D. R. Allan, *Phys. Rev. B* **48**, 16246 (1993).
- [31] S. Biering and P. Schwerdtfeger, *J. Chem. Phys.* **137**, 034705 (2012).
- [32] J. M. Ziman, *Electrons and Phonons* (Oxford University Press, London, 1960).
- [33] M. Omini and A. Sparavigna, *Phys. Rev. B* **53**, 9064 (1996).
- [34] W. Li, J. Carrete, N. A. Katcho, and N. Mingo, *Comput. Phys. Commun.* **185**, 1747 (2014).
- [35] G. Kresse and J. Furthmüller, *Phys. Rev. B* **54**, 11169 (1996).
- [36] D. M. Ceperley and B. J. Alder, *Phys. Rev. Lett.* **45**, 566 (1980).
- [37] P. E. Blöchl, *Phys. Rev. B* **50**, 17953 (1994); G. Kresse and D. Joubert, *ibid.* **59**, 1758 (1999).
- [38] U. Rössler, *New Data and Updates for Several Semiconductors with Chalcopyrite Structure, for Several II-VI Compounds and Diluted Magnetic IV-VI Compounds* (Springer, Berlin, Heidelberg, 2013).
- [39] A. Jain and A. J. H. McGaughey, *Comput. Mater. Sci.* **110**, 115 (2015).
- [40] W. Li, L. Lindsay, D. A. Broido, D. A. Stewart, and N. Mingo, *Phys. Rev. B* **86**, 174307 (2012).
- [41] W. Li, N. Mingo, L. Lindsay, D. A. Broido, D. A. Stewart, and N. A. Katcho, *Phys. Rev. B* **85**, 195436 (2012).
- [42] S. Radescu, A. Mujica, and R. J. Needs, *Phys. Rev. B* **80**, 144110 (2009); H. Kepa, T. Giebultowicz, B. Buras, B. Lebech, and K. Clausen, *Phys. Scr.* **25**, 807 (1982).
- [43] O. Madelung, *Data in Science and Technology: Semiconductors Other than Group IV Elements and III-V Compounds* (Springer-Verlag, Berlin, 1992).
- [44] A. Togo, F. Oba, and I. Tanaka, *Phys. Rev. B* **78**, 134106 (2008).
- [45] N. A. Spaldin, *J. Solid State Chem.* **195**, 2 (2012).
- [46] R. M. Pick, M. H. Chen, and R. M. Martin, *Phys. Rev. B* **1**, 910 (1970).
- [47] C. R. Whittsett and D. A. Nelson, *Phys. Rev. B* **5**, 3125 (1972).
- [48] T. Thonhauser, T. J. Scheidemantel, J. O. Sofo, J. V. Badding, and G. D. Mahan, *Phys. Rev. B* **68**, 085201 (2003).
- [49] S. V. Ovsyannikov and V. V. Shchennikov, *Chem. Mater.* **22**, 635 (2010).
- [50] L. Q. Xu, Y. P. Zheng, and J. C. Zheng, *Phys. Rev. B* **82**, 195102 (2010).
- [51] T. Ouyang and M. Hu, *J. Appl. Phys.* **117**, 245101 (2015).
- [52] F. Kelemen, E. Cruceanu, and D. Niculescu, *Phys. Status Solidi B* **11**, 865 (1965).
- [53] G. A. Slack, in *Solid State Physics*, edited by H. Ehrenreich, F. Seitz, and D. Turnbull (Academic, New York, 1979).
- [54] C. Toher, J. J. Plata, O. Levy, M. de Jong, M. Asta, M. B. Nardelli, and S. Curtarolo, *Phys. Rev. B* **90**, 174107 (2014).
- [55] L. Lindsay and D. A. Broido, *J. Phys.: Condens. Matter* **20**, 165209 (2008).
- [56] J. Callaway, *Phys. Rev.* **113**, 1046 (1959); D. T. Morelli, J. P. Heremans, and G. A. Slack, *Phys. Rev. B* **66**, 195304 (2002).
- [57] J. M. Rowe, R. M. Nicklow, D. L. Price, and K. Zanio, *Phys. Rev. B* **10**, 671 (1974).
- [58] X. Gu and R. Yang, *Appl. Phys. Lett.* **105**, 131903 (2014).
- [59] S. L. Shiné and J. S. Goela, *High Thermal Conductivity Materials* (Springer, Berlin, 2006).
- [60] L. M. Pavlova, A. S. Pashinkin, D. S. Gaev, and A. S. Pak, *High Temperature* **44**, 843 (2006).
- [61] H. M. Kagaya and T. Soma, *Phys. Status Solidi B* **138**, K13 (1986).
- [62] N. Vagelatos, D. Wehe, and J. S. King, *J. Chem. Phys.* **60**, 3613 (1974).
- [63] B. A. Weinstein, *Solid State Commun.* **24**, 595 (1977).
- [64] G. Ernst, C. Broholm, G. R. Kowach, and A. P. Ramirez, *Nature (London)* **396**, 147 (1998).
- [65] M. Blackman, *Philos. Mag.* **3**, 831 (1958).
- [66] N. Ashcroft and D. Mermin, *Solid State Physics* (Harcourt, New York, 1976).
- [67] J. M. Besson, P. Grima, M. Gauthier, J. P. Itié, M. Mézouar, D. Häusermann, and M. Hanfland, *Phys. Status Solidi B* **198**, 419 (1996).
- [68] B. N. Dutta, *Phys. Status Solidi* **2**, 984 (1962).
- [69] R. R. Reeber and K. Wang, *Mater. Chem. Phys.* **46**, 259 (1996).
- [70] C. H. Xu, C. Z. Wang, C. T. Chan, and K. M. Ho, *Phys. Rev. B* **43**, 5024 (1991).
- [71] P. Alers, H. E. Hintermann, and I. Hayward, *Thin Solid Films* **259**, 14 (1995).
- [72] J. Fabian and P. B. Allen, *Phys. Rev. Lett.* **79**, 1885 (1997).
- [73] G. A. Slack and P. Andersson, *Phys. Rev. B* **26**, 1873 (1982).
- [74] T. F. Smith and G. K. White, *J. Phys. C: Solid State Phys.* **8**, 2031 (1975).
- [75] B. L. Huang and M. Kaviany, *J. Appl. Phys.* **100**, 123507 (2006).